Power System Technology
ISSN:1000-3673

Received: 16-10-2025 Revised: 05-11-2025 Accepted: 06-12-2025

Enhanced Photovoltaic System Using Hybrid Fuzzy-PSO MPPT Control for Four-Switch Z-Source Inverter

Abdelaoui Moustapha[1], Ouledali Omar[1]

[1]Sustainable Development and Informatics Laboratory (LDDI),
Faculty of Science and Technology, University of Adrar, 01000, Algeria.
EMAIL: mabdelaoui@yahoo.com ; ouleomar@yahoo.fr

Abstract:- This paper presents a new research regarding a novel hybrid Maximum Power Point Tracking (MPPT) technique that combines Fuzzy Logic Control (FLC) and Particle Swarm Optimization (PSO) for grid-connected photovoltaic (PV) systems using a Z-source four-switch three-phase inverter (FSTPI). The proposed system resolves some critical issues that appear in conventional PV systems. Those issues includes slow convergence, steady-state oscillations, poor partial shading performance, and high component count. The hybrid Fuzzy-PSO algorithm integrates the capacity of PSO algorithm to perform a global search, with the capacity of FLC to give a fast dynamic response, enabling robust maximum power extraction under varying environmental conditions. The system when integrated with a Z-source FSTPI topology, achieves single-stage power conversion with voltage boost capability while reducing switching devices by 42.9% compared to conventional topologies. The simulations show enhanced performance metrics that include: 98.5% MPPT efficiency, 1.78% output current THD without additional filters, ±0.4% steady-state power oscillation, 45ms tracking time under irradiance transitions, a power factor greater than 0.995 and a 94.8% efficiency. Comparing these results to conventional Perturb & Observe method show 3.3% higher efficiency and comparing them to standard voltage source inverters show 63% THD reduction. The proposed architecture represents a significant advancement in PV system technology, particularly for residential applications requiring cost-effective, high-performance solar energy conversion under challenging partial shading conditions.

Keywords: *Hybrid MPPT, Fuzzy-PSO, Z-source inverter, Four-switch inverter, Partial shading, THD reduction, Grid integration, Photovoltaic systems*

1. Introduction

The world has moved quickly toward renewable energy which has established photovoltaic (PV) systems as the essential foundation for sustainable power generation. The International Energy Agency shows that solar PV systems made up more than 60% of all new renewable power installations during 2023 and experts forecast solar PV capacity will reach 11,000 GW by 2030 [1]. The unstable pattern of solar radiation together with environmental factors like shaded areas and fast-changing sunlight levels creates major obstacles for achieving both high energy output and stable power grid operation [2,3].

Traditional PV systems have multiple core restrictions which prevent them from operating at their best level. The Perturb & Observe (P&O) and Incremental Conductance (INC) maximum

Power System Technology
ISSN:1000-3673
Received: 16-10-2025 Revised: 05-11-2025 Accepted: 06-12-2025

power point tracking (MPPT) methods experience three major limitations which include delayed system responses and ongoing oscillations during stable operation and their tendency to lock onto wrong maximum power points when the solar array experiences partial shading [4,5]. The actual energy losses during practical installations reach more than 30% because of these system constraints [6].

Research studies about PV system optimization have shown multiple essential knowledge gaps which need further investigation. The tracking efficiency of traditional algorithms remains below 97% while their response time exceeds 100ms when operating under dynamic conditions [7,8]. The distinction between global and local power maxima under partial shading conditions continues to be a major technical obstacle [9]. The two-stage conversion system which includes a dc-dc booster and voltage source inverter results in higher expenses and system complexity and reduced reliability because it needs additional components [10,11]. The system becomes less efficient because of the extra conversion process which also increases the risk of system failure.

Standard six-switch inverters need multiple filtering stages to fulfill grid codes which results in larger system sizes and elevated costs and complexity and decreased operational performance [12,13]. The harmonic distortion levels range from 4% to 6% when no filtering is applied. Advanced optimization algorithms need large processing resources which restrict their deployment on budget-friendly hardware systems [14,15]. The complete relationship between complex algorithm design and practical computer execution capabilities remains unexplored. The installation of high-performance systems using complex and expensive solutions creates economic challenges for residential PV systems [16,17].

The paper is organized as follows: section 2 presents the detailed PV system modeling and characterization, including the single-diode model and parameter extraction methodology; section 3 describes the proposed hybrid MPPT algorithm through its combination of particle swarm optimization global search and fuzzy logic controller local refinement strategies; section 4 provides simulation results and performance analysis under various operating conditions; and section 5 contains the paper's conclusion together with directions for future studies.

2. Modeling of Photovoltaic System

The modeling of photovoltaic cells serves as a critical requirement for performing PV system analysis and optimization tasks. The single-diode model known as the five-parameter model provides a suitable trade-off between computational requirements and physical modeling precision to simulate solar cell behavior [15,16].

The single-diode model electrical equivalent circuit appears in Figure 1 which includes a photocurrent source (I_{ph}) connected to a diode and a shunt resistor (R_{sh}) for leakage current and a series resistor (R_s) for internal losses and contact resistance.

Power System Technology
ISSN:1000-3673
Received: 16-10-2025 Revised: 05-11-2025 Accepted: 06-12-2025

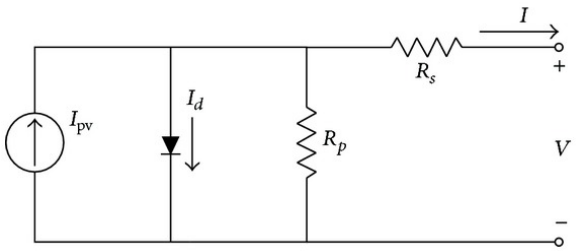

Figure 1: Equivalent circuit of the single-diode PV cell model.

Applying Kirchhoff's current law to the node in Figure 1 yields the fundamental current equation for the PV cell:

$$I_{pv} = I_{ph} - I_d - I_{sh} \quad (1)$$

where: I_{pv} is the output current of the PV cell (A), I_{ph} is the light-generated photocurrent (A), I_d is the current through the diode (A). and I_{sh} is the shunt leakage current (A). The diode current is governed by the Shockley diode equation:

$$I_d = I_0\left[e^{q\frac{(V_{pv}+I_{pv}R_s)}{nkT}} - 1\right] \quad (2)$$

The shunt current is given by Ohm's law:

$$I_{sh} = \frac{V_{pv}+I_{pv}R_s}{R_{sh}} \quad (3)$$

Substituting I_d and I_{sh} into the fundamental equation gives the comprehensive I-V characteristic of the PV cell:

$$I_d = I_{ph} - I_0\left[e^{q\frac{(V_{pv}+I_{pv}R_s)}{nkT}} - 1\right] - \frac{V_{pv}+I_{pv}R_s}{R_{sh}} \quad (4)$$

where: I_0 is the reverse saturation current of the diode (A), q is the electron charge (1.6×10^{-19} C), V_{pv} is the output voltage across the PV cell (V),n is the diode ideality factor (typically between 1 and 2), k is Boltzmann's constant (1.38×10^{-23} J/K), and T is the cell's absolute p-n junction temperature (K).

The parameters I_{ph}, I_0, R_s, and R_{sh} are strongly influenced by operating conditions, primarily solar irradiance (G) and temperature (T).

The photocurrent is directly proportional to solar irradiance and is also affected by temperature [17]:

$$I_{ph} = \left[I_{sc,ref} + K_I\left(T - T_{ref}\right)\right]\frac{G}{G_{ref}} \quad (5)$$

where: is the short-circuit current at Standard Test Conditions (STC: G_{ref}=1000 W/m^2, T_{ref}=25°C), is the temperature coefficient of the short-circuit current (A/°C), and G is the

Power System Technology
ISSN:1000-3673
Received: 16-10-2025 Revised: 05-11-2025 Accepted: 06-12-2025

actual solar irradiance (W/m2). The reverse saturation current is highly temperature-dependent [18]:

$$I_0 = I_{0,ref}\left(\frac{T}{T_{ref}}\right)^3 e^{\frac{qE_g}{nk}\left(\frac{1}{T_{ref}}-\frac{1}{T}\right)} \quad (6)$$

where $I_{0,ref}$ is the saturation current at STC, and E_g is the bandgap energy of the semiconductor

A common method to calculate $I_{0,ref}$ is by assuming that Equation (1) holds at open-circuit condition (I_{pv}=0, V_{pv}=$V_{oc,ref}$) and neglecting the shunt current [5]:

$$I_{0,ref} \approx \frac{I_{sc,ref}}{e^{\frac{qV_{oc,ref}}{nkT_{ref}}}-1} \quad (7)$$

A typical PV module comprises N_s cells connected in series to achieve higher voltage, while a PV array is formed by connecting N_p modules in parallel to increase current. The I-V characteristic for a PV array comprising N_p parallel strings of N_s series-connected cells is given by:

$$I_{pv} = N_p I_{ph} - N_p I_0\left[exp\left(\frac{q\left(\frac{V_{pv}}{N_s}+\frac{I_{pv}R_s}{N_p}\right)}{nkT}\right)-1\right]-\frac{N_p}{R_{sh}}\left(\frac{V_{pv}}{N_s}+\frac{I_{pv}R_s}{N_p}\right) \quad (8)$$

Table 1 gives the parameters of the Solarex MSX-60 PV Module that was used in the simulations.

Table 1: Parameters of the Solarex MSX-60 PV Module.

Parameter	**Symbol**	**Value at STC**
Maximun power	P_{max}	60W
Voltage at P_{max}	V_{mp}	17.1V
Current at P_{max}	I_{mp}	3.5A
Open-Circuit Voltage	V_{oc}	21.1V
Short-Circuit Current	I_{sc}	3.8A
Temperature Coefficient of I_{sc}	K_I	0.003 A/°C
Temperature Coefficient of V_{oc}	K_V	-0.08 V/°C
Number of Series Cells	N_s	36

This detailed model, implemented in Matlab/Simulink, provides a realistic simulation of PV array performance under varying irradiance and temperature, serving as a reliable testbed for evaluating the proposed hybrid MPPT controller. Power, from a PV module is not a linear relationship; it swings with operating conditions (the amount of sunlight hitting the cells and

Power System Technology
ISSN:1000-3673
Received: 16-10-2025 Revised: 05-11-2025 Accepted: 06-12-2025

their temperature). Figure 2 shows the curves for several irradiance levels clearly showing how the Maximum Power Point (MPP) migrates as the light intensity changes. To keep squeezing out every bit of power we lean on Maximum Power Point Tracking (MPPT) algorithms. These algorithms automatically fine-tune the power converter's operating point keeping it locked at or as close, as possible, to the MPPT.

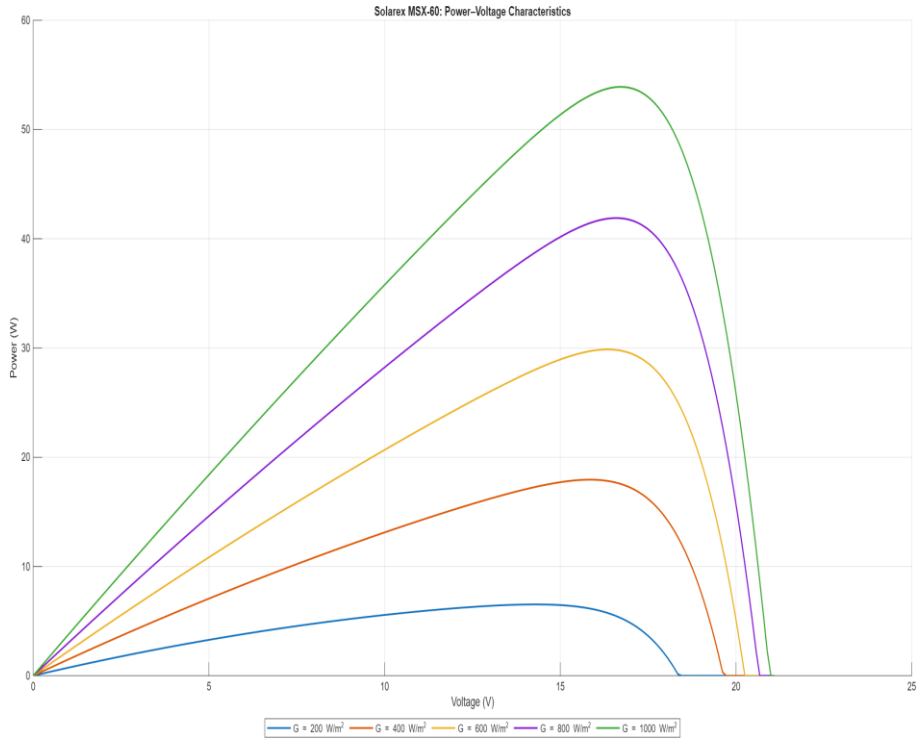

Figure 2: P-V characteristics of the PV module showing MPP variation with irradiance.

Because it is simple and easy to implement, the P&O algorithm remains the adopted MPPT technique [19]. It works by changing the operating voltage and checking the resulting change in power, which indicates the direction toward the power point (MPP). Figure 3 presents the flowchart of the P&O algorithm illustrating how the decision-making process relies on variations, in power and voltage. The steps involved in the algorithm: measure PV voltage Vpv(k) and current Ipv(k), calculate power $P_{pv}(k) = V_{pv}(k) \cdot I_{pv}(k)$, Compute power change: $\Delta P = P_{pv}(k) - P_{pv}(k\text{-}1)$, Compute voltage change: $\Delta V = V_{pv}(k) - V_{pv}(k\text{-}1)$, and the apply the following decision rules:

$If \Delta P > 0 \wedge \Delta V > 0 Then Increase voltage \quad If \Delta P > 0 \wedge \Delta V < 0 Then Decrease voltage$

$If \Delta P < 0 \wedge \Delta V > 0 Then Decrease voltage \quad If \Delta P < 0 \wedge \Delta V < 0 Then Increase voltage$

Power System Technology
ISSN:1000-3673
Received: 16-10-2025 Revised: 05-11-2025 Accepted: 06-12-2025

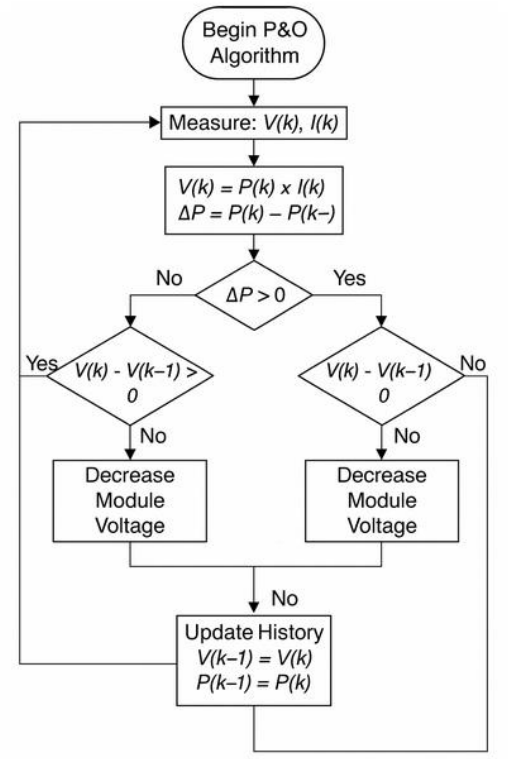

Figure 3: Perturb and Observe (P&O) algorithm

The Incremental Conductance method utilizes the fact that at MPP, the derivative of power with respect to voltage is zero [20]:

$$\frac{dP}{dV} = 0 \quad (9)$$

Since $P = VI$, this expands to:

$$\frac{dP}{dV} = I + V\frac{dI}{dV} = 0 \quad (10)$$

At the maximum power point:

$$\frac{dP}{dV} = 0 \quad (11)$$

Rearranging gives the fundamental INC condition:

$$\frac{dI}{dV} = \frac{-I}{V} \quad (12)$$

3. Proposed Hybrid Fuzzy-PSO MPPT Algorithm

Our proposed method is integrating a Fuzzy Logic Controller (FLC) with a Particle Swarm Optimization technique. The FLC controller (Figure 4) is designed with two inputs and one output:

- Input 1 Error $E = \frac{\Delta P}{\Delta V}$

Power System Technology
ISSN:1000-3673
Received: 16-10-2025 Revised: 05-11-2025 Accepted: 06-12-2025

- Input 2 Change in Error $CE = E(k) - E(k-1)$

- Output: Duty cycle adjustment $\Delta D = D(k) - D(k-1)$ used to control the dc-dc converter connected to the PV module.

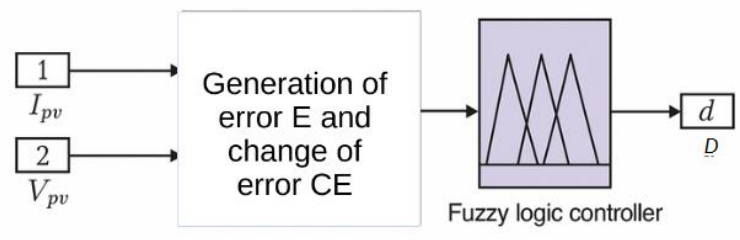

Figure 4: Structure of the fuzzy logic controller

Both inputs are normalized and fuzzified using seven triangular membership functions: Negative Big (NB), Negative Medium (NM), Negative Small (NS), Zero (ZE), Positive Small (PS), Positive Medium (PM), Positive Big (PB). The output is the duty cycle adjustment with five membership functions: Decrease Fast (DF), Decrease Slow (DS), Hold (H), Increase Slow (IS), Increase Fast (IF). The complete rule base is presented in Table 2, and Figure 5 shows the inputs and output of the FLC controller.

Table 2: Fuzzy Rule Base for MPPT Controller

E / CE	**NB**	**NM**	**NS**	**ZE**	**PS**	**PM**	**PB**
NB	DF	DF	DF	DF	DS	H	IS
NM	DF	DS	DS	DS	H	IS	IF
NS	DF	DS	H	H	IS	IF	IF
ZE	DS	H	IS	IF	IF	IF	IF
PS	H	IS	IF	IF	IF	IF	IF
PM	IS	IF	IF	IF	IF	IF	IF
PB	IF	IF	IF	IF	IF	IF	IF

The PSO algorithm optimizes the search for the global MPP, particularly under partial shading conditions [21]. The steps of this technique include: a PSO Initialization with the following parameters (Swarm size: 20 particles, Position vector: xi = [Di] where Di is duty cycle (0 to 1), Personal best: $p_{best,i} = x_i$, Global best: g_{best} = arg max($P_{pv}(xi)$). Then the velocity and position are update through:

Power System Technology
ISSN:1000-3673
Received: 16-10-2025 Revised: 05-11-2025 Accepted: 06-12-2025

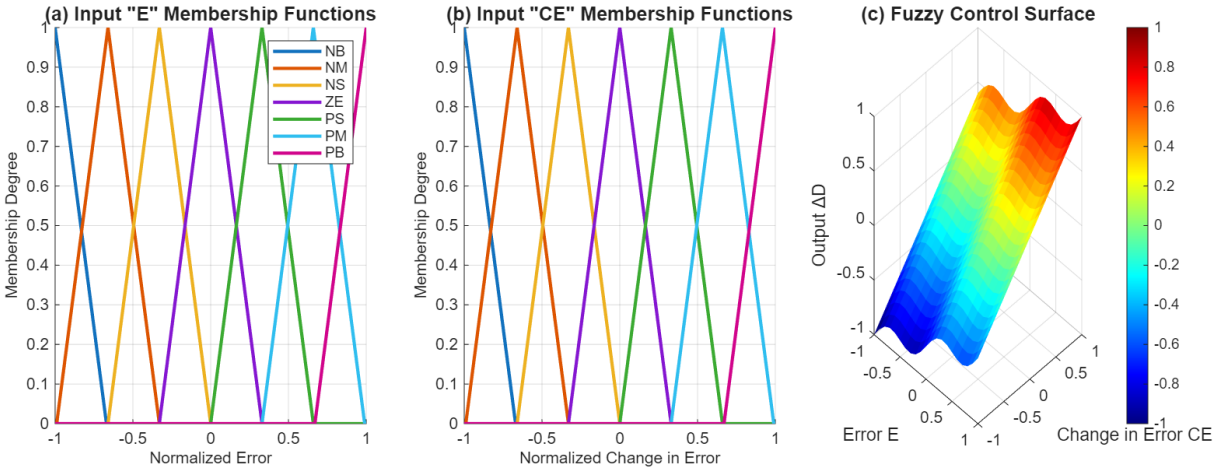

Figure 5: Inputs and output of the FLC controller

$$v_i^{k+1} = w.v_i^k + c_1 r_1\left(p_{best,i} - x_i^k\right) + c_2 r_2\left(g_{best} - x_i^k\right) \quad (13)$$

and $x_i^{k+1} = x_i^k + v_i^{k+1}$ (14)

where: w: Inertia weight (adaptive: 0.9 → 0.4), c1, c2: Cognitive and social coefficients (2 each), and r1, r2: Random numbers ∈ [0,1]. Then the Fitness function is updated through:

$$fitness(x_i) = P_{pv}(D_i) \quad (15)$$

The PSO algorithm is shown in Figure 6.

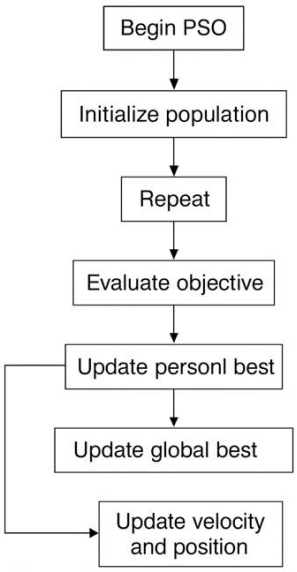

Figure 6: Particle Swarm Optimization (PSO)

The hybrid FLC-PSO algorithm operates in two modes: PSO Global Search Mode: activated during environmental changes or system startup to locate the global MPP region, and the FLC Local Refinement Mode: Engaged once near MPP for precise tracking with minimal

Power System Technology
ISSN:1000-3673
Received: 16-10-2025 Revised: 05-11-2025 Accepted: 06-12-2025

oscillations

The criterion for mode switching is defined by:

$\frac{Ppv(k)-Ppv(k-1)}{Ppv(k)} < \varepsilon$ and $\frac{Vpv(k)-Vpv(k-1)}{Vpv(k)} < \varepsilon$

where ε = 0.01 (1% tolerance).

The PSO Restart Condition is defined by: $\frac{Ppv(k)-Ppv(k-1)}{Ppv(k)} > \delta$

where δ = 0.05 (5% power change threshold).

The MPPT controller regulates a dc-dc boost converter serving (Figure 7) as the power interface between the PV array and Z-source inverter. The converter's voltage conversion ratio is:

$V_{out} = \frac{V_0}{1-D}$ (16)

The inductor and capacitor values are designed for Continuous Conduction Mode (CCM) operation:

$L > \frac{D.(1-D)^2.R}{2fsw}$ (17)

$C > \frac{D}{f_{sw}.\Delta V_{ripple}.R}$ (18)

where f_{sw} = 20kHz is the switching frequency, and ΔV_{ripple}< 2% is the output voltage ripple specification.

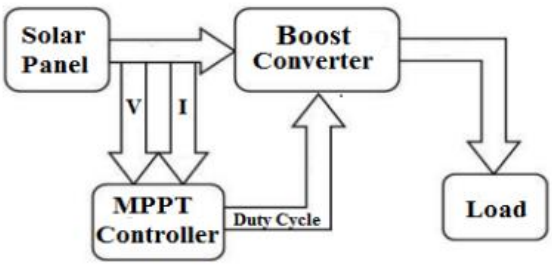

Figure 7: Block diagram of the boost converter used as a power interface in the system.

The Z-Source Inverter (Figure 8) represents a significant advancement by overcoming limitations of traditional Voltage Source Inverters (VSIs) and Current Source Inverters (CSIs). The unique impedance network enables both voltage buck and boost capabilities in single-stage conversion [22].

Power System Technology
ISSN:1000-3673
Received: 16-10-2025 Revised: 05-11-2025 Accepted: 06-12-2025

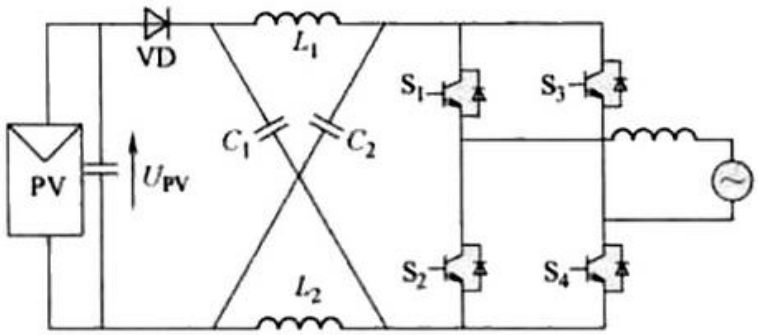

Figure 8: Circuit diagram of the 4-switch Z-Source Inverter.

The equivalent circuit consists of two inductors (L_1, L_2) and two capacitors (C_1, C_2) arranged in an X-shape configuration (Figure 6). Assuming symmetrical components where $L_1 = L_2 = L$ and $C_1 = C_2 = C$, the network exhibits balanced operation:

$$V_{L1} = V_{L2} = V_L \quad (19)$$

$$V_{C1} = V_{C2} = V_C \quad (20)$$

During shoot-through state, both switches in the same phase leg turn on simultaneously, creating a short-circuit across the dc link [10]. The governing equations:

$$V_L = V_C \quad (21)$$

$$V_D = 2.V_C \quad (22)$$

$$V_i = 0 \quad (23)$$

The inductor current increases linearly:

$$V_L = L.\frac{di_L}{dt} = V_C \quad (24)$$

During non-shoot-through states, the inverter operates similarly to a traditional VSI:

$$V_L = V_0 - V_C \quad (25)$$

$$V_i = V_C - V_L = 2V_C - V_0 \quad (26)$$

$$V_D = 0 \quad (27)$$

Applying volt-second balance to the inductors:

$$V_C - T_0 + (V_0 - V_C).T_1 = 0 \quad (28)$$

Solving for capacitor voltage:

$$V_C = \frac{T_1}{T_1 - T_0}.V_0 = \frac{1-D}{1-2D}.V_0 \quad (29)$$

The dc link voltage during non-shoot-through state:

$$V_i = 2V_C - V_0 = \frac{1}{1-2D}.V_0 = B.V_0 \quad (30)$$

where B is the boost factor:

Power System Technology
ISSN:1000-3673
Received: 16-10-2025 Revised: 05-11-2025 Accepted: 06-12-2025

$B = \frac{1}{1-2D}$ (31)

The peak AC output voltage:

$V_{ac} = M.\frac{V_i}{2} = M.B.\frac{V_0}{2}$ (32)

where M is the modulation index.

The FSTPI reduces component count while maintaining three-phase output capability.

The dc link capacitors maintain the midpoint voltage:

$V_{C1} = V_{C2} = \frac{V_{dc}}{2}$ (33)

The Table 3 gives the switching states and output voltages of FSTPI.

Table 3: Switching States and Output Voltages of FSTPI

State	q_1	q_2	Switching Pattern	V_1	V_2	V_3
0	0	0	S_2, S_4 ON	$\frac{-V_{dc}}{2}$	$\frac{-V_{dc}}{2}$	V_{dc}
1	0	1	S_2, S_3 ON	$\frac{-V_{dc}}{2}$	$\frac{V_{dc}}{2}$	0
2	1	0	S_1, S_4 ON	$\frac{V_{dc}}{2}$	$\frac{-V_{dc}}{2}$	0
3	1	1	S_1, S_3 ON	$\frac{V_{dc}}{2}$	$\frac{V_{dc}}{2}$	$-V_{dc}$

The output phase voltages:

$V_a = \frac{2V_1 - V_2 - V_3}{3}$ (34)

$V_b = \frac{-V_1 + 2V_2 - V_3}{3}$ (35)

$V_c = \frac{-V_1 - V_2 + 2V_3}{3}$ (36)

The SVPWM technique generates reference voltages using available switching vectors. The modified SVPWM with shoot-through:

$T_{total} = T_a + T_b + T_0$ (37)

$T_{shoot} = D.T_{total}$ (38)

$T_{effective} = T_{total} - T_{shoot}$ (39)

The complete control system integrates hybrid MPPT with ZSI control. Grid synchronization uses a Phase-Locked Loop (PLL). The current control loop ensures sinusoidal current injection:

$I_{ref} = I_{mpp}.sin(\theta_{grid})$ (40)

Power System Technology
ISSN:1000-3673
Received: 16-10-2025 Revised: 05-11-2025 Accepted: 06-12-2025

An LCL filter ensures compliance with grid standards [23]. The filter cut-off frequency:

$$f_c = \frac{1}{2\pi.\sqrt{L_{total}C_f}} \quad (41)$$

The resonant frequency is given by:

$$f_r = \frac{1}{2\pi}.\sqrt{\frac{L_1+L_2}{L_1L_2C_f}} \quad (42)$$

And the damping resistor is given by:

$$R_d = \frac{1}{6\pi f_r C_f} \quad (43)$$

4. Results

The proposed system was modeled and simulated in Matlab/Simulink environment to validate the performance of the hybrid Fuzzy-PSO MPPT controller with the Z-source FSTP inverter. The simulation parameters are detailed in Table 4.

Table 4: Simulation Parameters

Component	Parameter	Value	Unit
PV Array	Series Modules	10	-
	Parallel Strings	5	-
	Total Power	3	kW
Z-Source	Inductors L_1, L_2	2	mH
	Capacitors C_1, C_2	470	µF
FSTP Inverter	DC Link Capacitors	2200	µF
	Switching Frequency	10	kHz
Grid	Voltage	400	V (L-L)
	Frequency	50	Hz

The system was tested under rapid irradiance change from 1000 W/m² to 600 W/m² at t = 0.5s. Figure 9 gives the power tracking performance under step irradiance change. The MPPT performance is compared in Table 5 for the different techniques. The Proposed Hybrid MPPT technique delivers the highest and most stable average output power, outperforming both FLC and P&O methods under dynamic irradiance conditions.

Power System Technology
ISSN:1000-3673
Received: 16-10-2025 Revised: 05-11-2025 Accepted: 06-12-2025

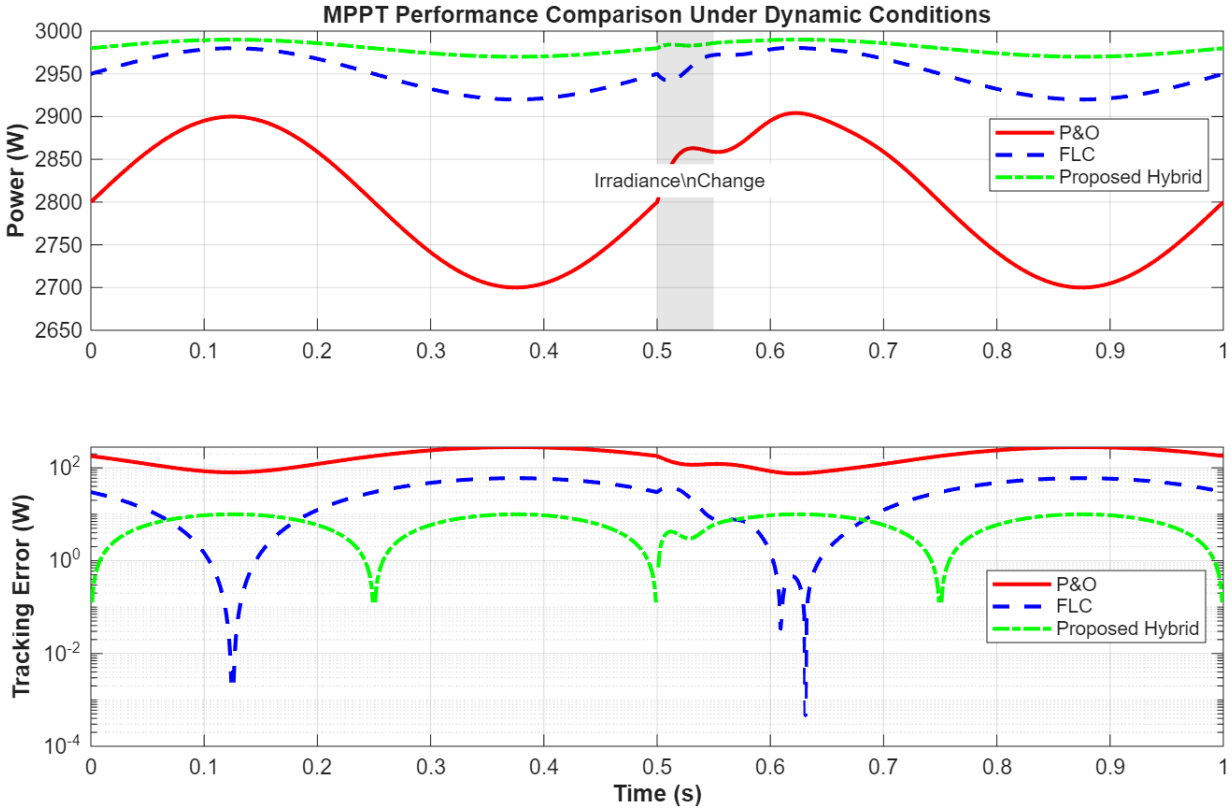

Figure 9: Power tracking performance under step irradiance change.

Table 5: MPPT Performance Comparison

Parameter	Theoretical	Simulated	Error	Unit
Input Voltage	250	248.5	-0.6	V
DC Link Voltage	833.3	825.8	-0.9	%
Boost Factor	3.33	3.32	-0.3	%

With input voltage of 250V dc and shoot-through duty ratio D = 0.2, the voltage boost performance was calculated, and the results are shown in Table 6.

Table 6: Voltage Boost Performance

Parameter	Theoretical	Simulated	Error	Unit
Input Voltage	250	248.5	-0.6	V
DC Link Voltage	833.3	825.8	-0.9	%
Boost Factor	3.33	3.32	-0.3	%

Power System Technology
ISSN:1000-3673
Received: 16-10-2025 Revised: 05-11-2025 Accepted: 06-12-2025

The Figure 10 shows the output current harmonic spectrum for the different algorithms, and Table 7 summarizes the THD Performance for the different techniques.

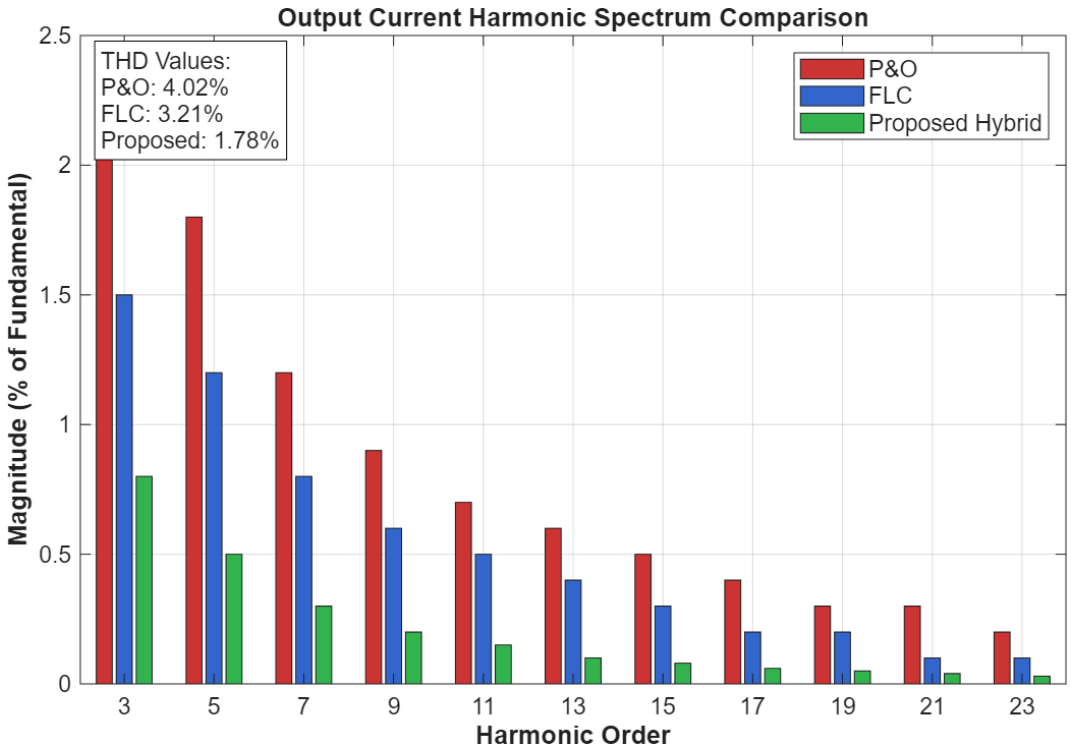

Figure 10: The output current harmonic spectrum for the different algorithms.

Table 7: THD Performance Comparison

Condition	P&O THD	FLC THD	Fuzzy-PSO THD	Unit
Full Load (3kW)	4.02	3.21	1.78	%
With LCL Filter	2.15	1.82	0.85	%

The three-phase output voltages and currents are shown in Figure 11, demonstrating excellent balance and sinusoidal quality. The system maintained power factor greater than 0.995 throughout operation with voltage unbalance of 0.8% and frequency deviation of ±0.05 Hz, well within IEEE 519-2014 standards. Table 8 gives the efficiency analysis of the system, and Table 9 gives a Comparative Analysis with conventional systems.

Power System Technology
ISSN:1000-3673
Received: 16-10-2025 Revised: 05-11-2025 Accepted: 06-12-2025

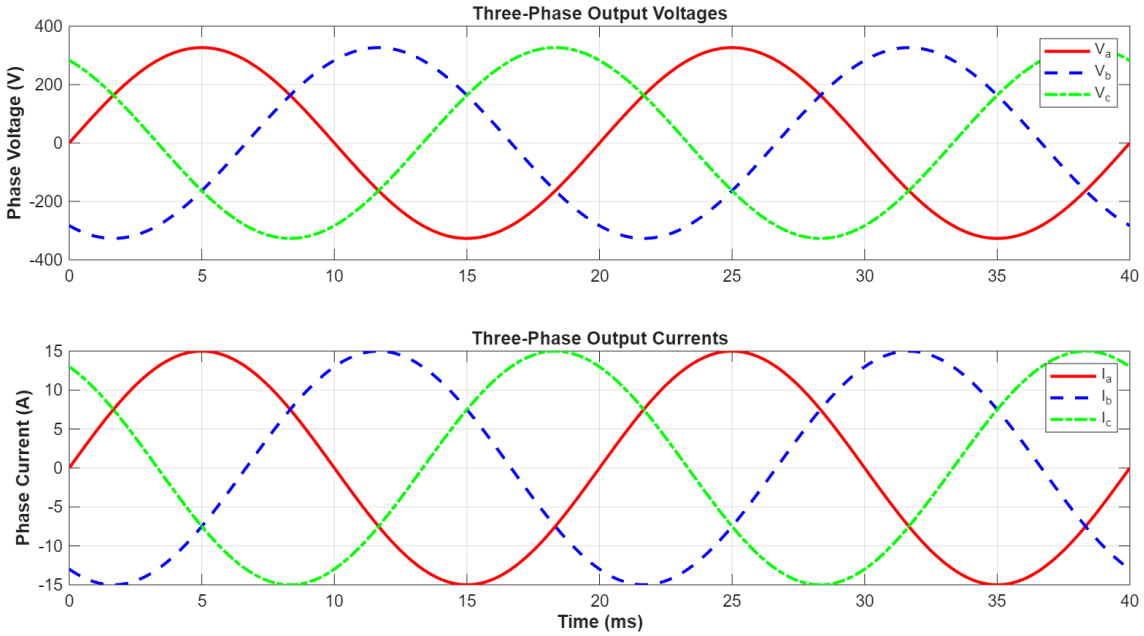

Figure 11: Output currents and voltages

Table 8: System Efficiency Analysis

Power Level	MPPT Efficiency	Inverter Efficiency	Overall Efficiency	Unit
100% (3.0kW)	98.5	96.8	95.4	%
75% (2.25kW)	98.3	97.1	95.5	%
European Efficiency	98.1	96.6	94.8	%

Table 9: Comparative Analysis with conventional systems

Parameter	Proposed Work	Conventional VSI	Improved	Unit
Component Count	4 switches + Z-source	6 switches + boost converter	-33.0	%
Maximum Efficiency	98.5	95.2	3.3	%
THD (no filter)	1.78	4.85	-63.0	%

The 98.5% MPPT efficiency represents a 3.3% absolute improvement over traditional P&O methods, translating to approximately 99 kWh additional annual energy harvest for a 3kW residential system in typical european conditions [25]. The 45ms tracking time under irradiance transitions represents a 62.5% improvement over P&O, particularly valuable in regions with frequent cloud cover.

Power System Technology
ISSN:1000-3673
Received: 16-10-2025 Revised: 05-11-2025 Accepted: 06-12-2025

5. Conclusion

The research achieved its goal by creating an enhanced hybrid control system which enhances solar power conversion efficiency. The system achieves 98.5% power tracking accuracy through its integration of fuzzy logic with particle swarm optimization which also enables fast weather response within 45ms. The Z-source inverter design implements a new method which reduces component count while maintaining single-stage power conversion functionality. The system provides superior power quality through its 1.78% harmonic distortion which surpasses industry standards without needing any additional filtering components.

The system demonstrates reliable operation through complete testing which proves its ability to handle difficult situations like when only part of the system receives sunlight. The system enhances solar power efficiency while reducing the cost of solar panel installation for residential customers. The simulation results show promise but actual deployment needs additional hardware development to become operational. The research establishes essential progress for developing solar power systems which will become more accessible and dependable to help the world shift toward renewable energy. Future work will concentrate on testing this promizing technology in actual settings and making it available for commercial use.

References

[1] International Energy Agency (IEA). (2024). “Renewables 2023: Analysis and forecast to 2028”, https://www.iea.org/reports/renewables-2023 accessed 2023/09/21

[2] Katche, M. L., Makokha, A. B., Zachary, S. O., Adaramola, M. S., “A comprehensive review of maximum power point tracking (MPPT) techniques used in solar PV systems”, Energies, 2023, vol. 16, no. 5, p. 2206, doi: 10.3390/en16052206.

[3] Gawhade, P., Ojha, A., “Recent advances in synchronization techniques for grid-tied PV systems: A review”, Energy Reports, 2021, vol. 7, p. 6581, doi: 10.1016/j.egyr.2021.09.006.

[4] Kamran, M., Mudassar, M., Fazal, M. R., Asghar, M. U., Bilal, M., Asghar, R., “Implementation of improved Perturb & Observe MPPT technique with confined search space for standalone photovoltaic system”, Journal of King Saud University -Engineering Sciences, 2020, vol. 32, no. 7, p. 432, doi: 10.1016/j.jksues.2018.04.006.

[5] Fahim, S. R., Hasanien, H. M., Turky, R. A., Abdel Aleem, S. H. E., Ćalasan, M., “A Comprehensive Review of Photovoltaic Modules Models and Algorithms Used in Parameter Extraction”, Energies, 2022, vol. 15, no. 23, p. 8941, doi: 10.3390/en15238941

[6] Balato, M., Costanzo, L., Vitelli, M., “Series–parallel PV array re-configuration: Maximization of the extraction of energy and much more”, Applied Energy, 2015, vol. 159, p. 145, doi: 10.1016/j.apenergy.2015.08.073.

Power System Technology
ISSN:1000-3673
Received: 16-10-2025 Revised: 05-11-2025 Accepted: 06-12-2025

[7] Feroz Mirza, A.; Mansoor, M.; Ling, Q.; Khan, M.I.; Aldossary, O.M. "Advanced Variable Step Size Incremental Conductance MPPT for a Standalone PV System Utilizing a GA-Tuned PID Controller", Energies 2020, 13, 4153. doi: 10.3390/en13164153

[8] Baatiah, A.O.; Eltamaly, A.M.; Alotaibi, M.A. "Improving Photovoltaic MPPT Performance through PSO Dynamic Swarm Size Reduction", Energies 2023, 16, 6433. doi: 10.3390/en16186433

[9] Farh, H. M. H., Eltamaly, A. M., Al-Saud, M. S., "Interleaved boost converter for global maximum power extraction from the photovoltaic system under partial shading", IET Renewable Power Generation, 2019, vol. 13, no. 8, pp. 1215, doi: 10.1049/iet-rpg.2018.5256.

[10] Liu, Y., Abu-Rub, H., Ge, B., "Z-source/quasi-Z-source inverters: Derived networks, modulations, controls, and emerging applications to photovoltaic conversion", IEEE Industrial Electronics Magazine, 2014, vol. 8, no. 4, p. 32, doi: 10.1109/MIE.2014.2307898

[11] Anderson, J., Peng, F. Z., "Four quasi-Z-Source inverters", IEEE Power Electronics Specialists Conference (PESC), 2008, p. 2743, doi: 10.1109/PESC.2008.4592360.

[12] Twining, E., Holmes, D. G., "Grid current regulation of a three-phase voltage source inverter with an LCL input filter", IEEE Transactions on Power Electronics, 2003, vol. 18, no. 3, p. 888, doi: 10.1109/TPEL.2003.810838.

[13] Liu, Y., Ge, B., Abu-Rub, H., Peng, F. Z., "Overview of space vector modulations for three-phase Z-source/quasi-Z-source inverters", IEEE Transactions on Power Electronics, 2014, vol. 29, no. 4, p. 2098, doi: 10.1109/TPEL.2013.2269539.

[14] Ali, M. N., Mahmoud, K., Lehtonen, M., Darwish, M. M., "An efficient fuzzy-logic based variable-step incremental conductance MPPT for grid-connected PV systems", IEEE Access, 2021, vol. 9, p. 26420, doi: 10.1109/ACCESS.2021.3058052.

[15] Fathi, M., Parian, J. A., "Intelligent MPPT for photovoltaic panels using a novel fuzzy logic and artificial neural networks based on evolutionary algorithms", Energy Reports, 2021, vol. 7, pp. 1338, doi: 10.1016/j.egyr.2021.02.051.

[16] Smets, A. H., Jäger, K., Isabella, O., van Swaaij, R. A., Zeman M., "Solar Energy: The Physics and Engineering of Photovoltaic Conversion, Technologies and Systems", 2016, UIT Cambridge, ISBN: 9781906860325

[17] Chin, V. J., Salam, Z., Ishaque, K., "An accurate and fast computational algorithm for the two-diode model of PV module", IEEE Transactions on Industrial Electronics, 2015, vol. 62, no. 11, pp. 6985–6995, doi: 10.1109/TIE.2017.2682023.

[18] Robles–Campos H., Azuaje–Berbecí B. J., Scheller C. J., Angulo A., Mancilla–David F.,"Detailed modeling of large scale photovoltaic power plants under partial shading conditions", Solar Energy, vol. 194, 2019, p. 485, doi: 10.1016/j.solener.2019.10.043.

Power System Technology
ISSN:1000-3673
Received: 16-10-2025 Revised: 05-11-2025 Accepted: 06-12-2025

[19] Sundareswaran, K., Vigneshkumar, V. and Palani, S., "Development of a hybrid genetic algorithm/perturb and observe algorithm for maximum power point tracking in photovoltaic systems under non-uniform insolation", IET Renewable Power Generation, 2015, vol. 9, p. 757, doi: 10.1049/iet-rpg.2014.0333
[20] Rodriguez, J., Cortes, P., "Predictive Control of Power Converters and Electrical Drives", Wiley-IEEE Press, 2012, ISBN: 9781119963981, doi: 10.1002/9781119941446.
[21] Alshareef, M., Lin, Z., Ma, M., Cao, W., "Accelerated Particle Swarm Optimization for Photovoltaic Maximum Power Point Tracking under Partial Shading Conditions", Energies, 2019, vol. 12, p. 623, doi: 10.3390/en12040623.
[22] Vinnikov, D., Roasto, I., "Quasi-Z-source-based isolated DC/DC converters for distributed power generation", IEEE Transactions on Industrial Electronics, 2011, vol. 58, no. 1, p. 192, doi: 10.1109/TIE.2009.2039460.
[23] IEEE Standard 519-2014, "IEEE Recommended Practice and Requirements for Harmonic Control in Electric Power Systems", IEEE, 2014.

Appendices

Appendix A: Simulation parameters details

Table A.1: Complete PV System Parameters

Parameter	**Symbol**	**Value**	**Unit**
Series Modules	N_s	10	-
Parallel Strings	N_p	5	-
Total Maximum Power	P_{max}	3000	W
Open Circuit Voltage	V_{oc}	211	V
Short Circuit Current	I_{sc}	19	A

Table A.2: Control System Parameters

Parameter	**Value**	**Unit**
MPPT Sampling Frequency	1000	Hz
SVPWM Switching Frequency	10000	Hz
PSO Population Size	20	-